AD-A118 791 AIR FORCE GEOPHYSICS LAB HANSCOM AFB MA F/G 22/2
HIGH-LEVEL SPACECRAFT CHARGING ENVIRONMENTS NEAR GEOSYNCHRONOUS--ETC(U)
FEB 82 E G MULLEN, M S GUSSENHOVEN
UNCLASSIFIED AFGL-TR-82-0063 NL

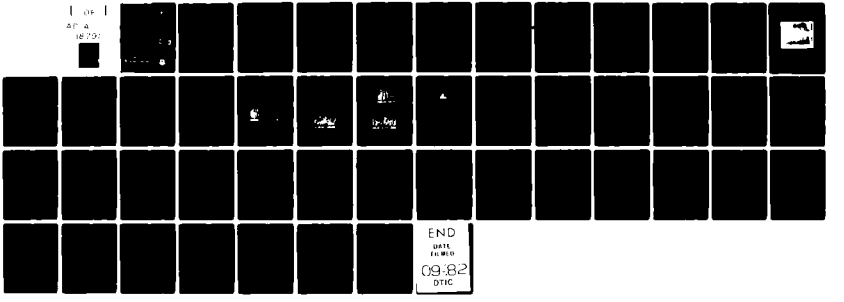

AFGL-TR-82-0063
ENVIRONMENTAL RESEARCH PAPERS, NO. 771

High-Level Spacecraft Charging Enviroments Near Geosynchronous Orbit

E.G. MULLEN
M.S. GUSSENHOVEN

11 FEBRUARY 1982

SPACE PHYSICS DIVISION PROJECT 7661
AIR FORCE GEOPHYSICS LABORATORY
HANSCOM AFB, MASSACHUSETTS 01731

AIR FORCE SYSTEMS COMMAND, USAF

This report has been reviewed by the ESD Public Affairs Office (PA) and is releasable to the National Technical Information Service (NTIS).

This technical report has been reviewed and is approved for publication.

Alva T. Stair, Jr.

DR. ALVA T. STAIR, Jr
Chief Scientist

Qualified requestors may obtain additional copies from the Defense Technical Information Center. All others should apply to the National Technical Information Service.

Unclassified

SECURITY CLASSIFICATION OF THIS PAGE (When Data Entered)

REPORT DOCUMENTATION PAGE		READ INSTRUCTIONS BEFORE COMPLETING FORM
1. REPORT NUMBER AFGL-TR-82-0063	2. GOVT ACCESSION NO. AD-A118 791	3. RECIPIENT'S CATALOG NUMBER
4. TITLE (and Subtitle) HIGH-LEVEL SPACECRAFT CHARGING ENVIRONMENTS NEAR GEOSYNCHRONOUS ORBIT		5. TYPE OF REPORT & PERIOD COVERED Scientific. Interim. 6. PERFORMING ORG. REPORT NUMBER ERP No. 771
7. AUTHOR(s) E.G. Mullen M.S. Gussenhoven*		8. CONTRACT OR GRANT NUMBER(s)
9. PERFORMING ORGANIZATION NAME AND ADDRESS Air Force Geophysics Laboratory (PHG) Hanscom AFB Massachusetts 01731		10. PROGRAM ELEMENT, PROJECT, TASK AREA & WORK UNIT NUMBERS 62101F 76610803
11. CONTROLLING OFFICE NAME AND ADDRESS Air Force Geophysics Laboratory (PHG) Hanscom AFB Massachusetts 01731		12. REPORT DATE 11 February 1982 13. NUMBER OF PAGES 47
14. MONITORING AGENCY NAME & ADDRESS(if different from Controlling Office)		15. SECURITY CLASS. (of this report) Unclassified 15a. DECLASSIFICATION DOWNGRADING SCHEDULE

16. DISTRIBUTION STATEMENT (of this Report)

Approved for public release; distribution unlimited.

17. DISTRIBUTION STATEMENT (of the abstract entered in Block 20, if different from Report)

18. SUPPLEMENTARY NOTES

*Boston College, Chestnut Hill, Massachusetts

19. KEY WORDS (Continue on reverse side if necessary and identify by block number)

Spacecraft charging	Ions
SCATHA	Electrons
Space environment	Space physics
Energetic particles	

20. ABSTRACT (Continue on reverse side if necessary and identify by block number)

High-level spacecraft charging events in sunlight are discussed and statistically analyzed to determine environmental parameters critical to charging and the region of space near geosynchronous altitude where charging occurs. Significant levels of spacecraft charging are shown to occur only between 1900 LT and 0900 LT at any altitude or latitude of the SCATHA satellite orbit. High-level charging is shown to occur only during periods when the magnetic activity index K_p is 2+ or greater. Distribution functions

DD FORM 1 JAN 73 1473

Unclassified

SECURITY CLASSIFICATION OF THIS PAGE (When Data Entered)

20. (contd)

of energetic electrons and ions are presented for 3 high-level charging periods on days 114, 241 and 363, 1979. Moments of the distribution functions are determined, and fitting techniques used to derive two-Maxwellian densities and temperatures are discussed. Results are provided in a format usable in satellite design specifications.

Preface

The authors would like to thank the SCATHA experimenters: D. A. Hardy, AFGL; T. L. Aggson, NASA Goddard; B. G. Ledley, NASA Goddard; E. C. Whipple, UCSD; P. F. Mizera, Aerospace; J. F. Fennell, Aerospace; R. G. Johnson, Lockheed; J. B. Reagan, Lockheed; H. C. Koons, Aerospace, and R. C. Adamo, SRI for use of their data and the countless discussions of its interpretation. Special thanks are given to D. E. Delorey of Boston College who endured numerous computer program modifications to give us a quality product and his contract monitor, Mr. R. E. McInerney of AFGL who provided us the necessary computer resources to accomplish the task. Special thanks are also given to J. Feynman of Boston College for use of her statistical survey of the SC5 particle fluxes. Thanks are also given to N. Heinemann and M. Wilcox-Totten of Boston College for data presentations, L. Cassidy and B. McKee of Regis College for graphics and artwork, and J. Cronin of AFGL for his computer graphics and statistical analysis. The work of M. S. Gussenhoven was supported by the Air Force Geophysics Laboratory under Contract F19628-82-K-0011.

Contents

Illustrations

Illustrations

Tables

Tables

High-Level Spacecraft Charging Environments Near Geosynchronous Orbit

1. INTRODUCTION

This report is a continuation of the work begun by Mullen et al[1] to document a "worst case" environment in the near-geosynchronous regime and to define the region where this environment may be encountered. Results of this study are discussed in a manner that is consistent with requirements to provide the necessary revision material for MIL STD 1541.

Much of the methodology, statistical calculations, and so on, discussed in Mullen et al[1] is not repeated here. Only new techniques and results are elaborated on. The report consists of several sections. The first demonstrates the validity of using SC10 to measure spacecraft charging in sunlight. Since many people presently working in the field are somewhat skeptical of the technique, we show that our data set is valid before proceeding to the analysis. Next we show some of the charging variations and their associated time intervals as seen on SCATHA. This is followed by the charging statistics, which show the region of space near geosynchronous altitude where charging is most likely to occur and the approximate frequency of occurrence. (Results are from a data set that is limited to 1 year.)

(Received for publication 10 February 1982)

1. Mullen, E.G., Gussenhoven, M.S., and Garrett, H.B. (1981) A "Worst Case" Spacecraft Environment as Observed by SCATHA on 24 April 1979, AFGL-TR-81-0231, AD A108680.

The next section begins the "worst case" studies. Three days are closely examined: days 114, 241, and 363 from 1979. The magnetospheric conditions, particle populations, distribution functions, and charging levels are discussed. In summary, we discuss the environmental parameters felt to be most critical to spacecraft charging.

2. MEASUREMENTS OF SPACECRAFT CHARGING

Spacecraft charging in this report refers to plasma-to-vehicle-frame potential difference (ϕ_f) unless otherwise specifically stated. Traditionally, spacecraft charging levels at synchronous orbit have been determined from particle detector measurements on the satellite (see DeForest[2]). Spectrograms of the data show charging peaks in the ions at the vehicle charging potential. A sample spectrogram showing sunlight charging between ~1600 UT and 1900 UT on day 241, 1979 is shown in Figure 1. The use of particle detectors to determine vehicle charging has some drawbacks. First, particle detectors are not placed on satellites with detection of vehicle charging as their prime mission. Therefore, their energy channel widths, energies and sampling intervals are often not optimal for studying spacecraft charging, especially lower level sunlight charging. Second, for some low-level charging events, ion flux returns are preferentially magnetic-field-aligned, and unless the particle detector samples in the right direction at the right energy a charging peak will not show in the data.

The SC10 instrument on the SCATHA satellite consists of a 100 m tip-to-tip dipole antenna configuration with the inner 30-m sections of the 50-m antennas coated with Kapton insulation. (See Stevens and Vampola[3] for further information.) One of the measurements made by SC10 is a common mode voltage between one of the 50-m antennas and spacecraft ground. This measurement in sunlight is the spacecraft frame potential ϕ_f and has a time resolution of 2 points per sec, thus providing an excellent data base for studying charging effects. Figure 2 is a plot of ϕ_f as determined from ion peaks measured by the SC9 particle spectrometer on SCATHA versus ϕ_f as measured by SC10. A reference line is drawn at 45° to show where equality occurs. The data are from the 3 "worst case" days used in this study:

2. DeForest, S. E. (1972) Spacecraft charging at synchronous orbit, JGR, 77:651-659
3. Stevens, J. R., and Vampola, A. L. (Eds.) (1978) Description of the Space Test Program P78-2 Spacecraft and Payloads, SAMSO-TR-78-24.

days 114, 241, and 363, 1979. Table 1 gives the number of points (n) from each day and the correlation coefficients (r) of a linear regression performed with the two sets of values. A spot comparison of charging values on other days gave the same results.

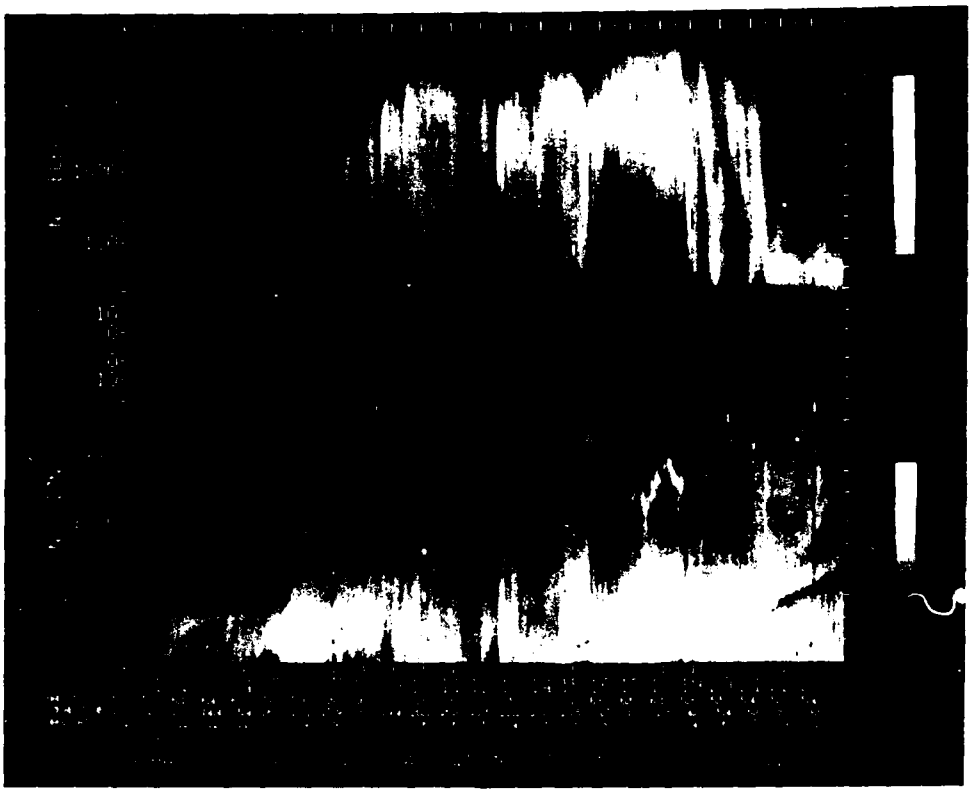

Figure 1. Spectrogram of the SCP Particle Counts for Day 241, 1979 Showing the Ion Peak During Sunlight Charging Between ~1600 U.T. and 1900 U.T. Energy is plotted along the x-axis with electrons at the top and ions at the bottom.

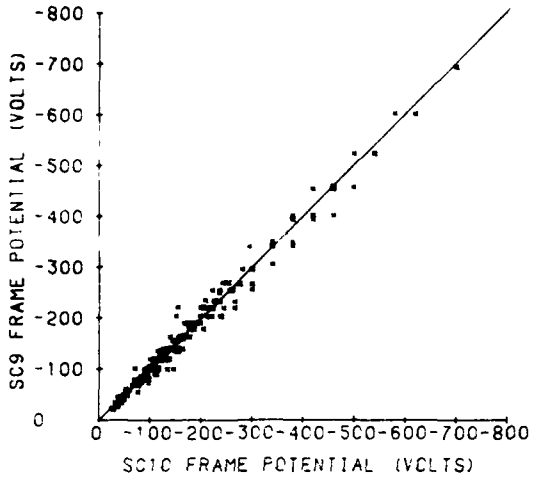

Figure 2. Mass Plot of SC9 Frame Potential ϕ_f as Determined From Ion Peaks Versus SC10 Frame Potential ϕ_f as Measured by the Common Mode Voltage for Simultaneous Times on Days 114, 241, and 363, 1979

Table 1. SC9 Versus SC10 Charging Comparison Statistics

Day	n	r
114	125	0.98
241	68	0.99
363	57	0.99
Total	250	0.99

Some of the small differences between SC9 and SC10 values are due to the inability to pick the exact channel of the ion peak (no interpolation was performed). Also, SC10 measurements above 300 V only have a resolution of 40 V. Extreme care must be used in identifying the exact time of the charging peak in the particle detector data since the vehicle potential changes very rapidly with both sun angle and environment. This is demonstrated in Figure 3 which shows a plot of 1-sec values of ϕ_f as measured by SC10 between 1928 UT and 1932 UT on day 363, 1979. Superimposed on the plot are values of ϕ_f as determined from the SC9 particle detectors for the same period. Two types of variations can be seen, a spin variation peaking once per spin (arrows) due to boom configurations and surface materials facing the sun at any particular time, and changes in levels between and within spins due to changes in the ambient particle environment. This plot shows that using particle detector data to determine ϕ_f for a statistical study could be misleading

since points from the same 16-sec energy scan interval can give different (but correct) values of ϕ_f. Spin-sun angle effects are also shown in Figures 2 and 3 of Mullen et al. [1] To determine temporal variations in ϕ_f independent of material properties, sun angle, and so on, ϕ_f is represented by its maximum value within a small Δt near the same satellite-sun orientation each spin (arrows in Figure 3). This value is nearly always the maximum value for the spin. The only exceptions occur when the particle environment is changing extremely fast within a spin period. The charging statistics which follow use only the spin maximums taken from the same spin-sun angle each spin period.

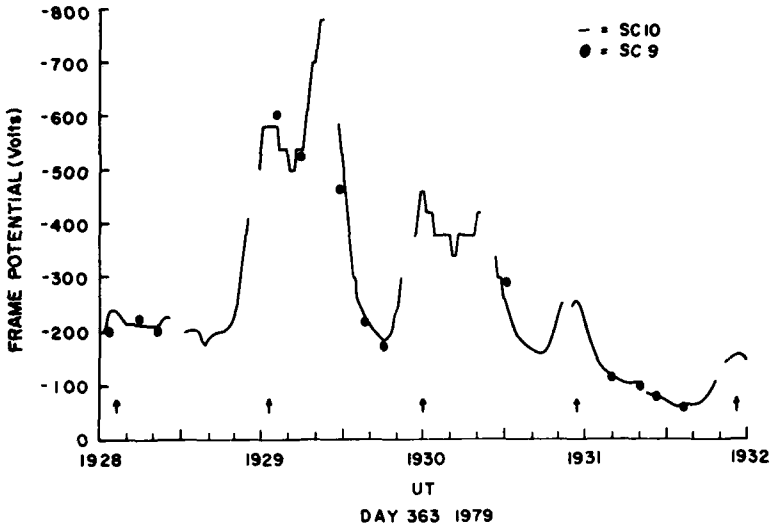

Figure 3. One-second Values of Frame Potential ϕ_f as Measured by SC10 (line) Between 1928 UT and 1932 UT on Day 363, 1979, and as Determined from SC9 Ion Peaks (●) for the Same Period. Arrows indicate times of normal spin/sun angle maximums

3. FRAME CHARGING STATISTICS

Sixty-nine days of data between day 81, 1979 and day 46, 1980 are used as the sample data base. The 69 days are days from the original 75 Atlas days when SC10 data were available. The days used are listed in Table 2. The maximum charging value for each spin is used, and the data are edited to eliminate beam operations,

satellite eclipse periods and noise spikes. The final data base consists of 95,918 data points. Their distributions in local time, L-shell, and K_p are given in Tables 3, 4, and 5.

Table 2. Days Included in Charging Statistics Data Base

Year-Day	Year-Day	Year-Day	Year-Day	Year-Day
79-81	79-121	79-178	79-272	79-351
-87	-127	-180	-273	-357
-88	-138	-188	-278	-359
-90	-142	-200	-279	-361
-91	-144	-206	-280	-363
-93	-145	-216	-281	80-4
-94	-146	-225	-282	-18
-95	-149	-232	-301	-27
-103	-156	-241	-311	-28
-110	-158	-254	-317	-36
-111	-160	-261	-328	-37
-114	-164	-262	-329	-42
-115	-166	-264	-331	-46
-120	-172	-271	-341	

Table 3. SC10 Data Base Versus Local Time

Local Time	Number of Points	Number of Days	Local Time	Number of Points	Number of Days
0000-0100	3445	64	1200-1300	4015	67
0100-0200	4168	66	1300-1400	3939	66
0200-0300	4166	67	1400-1500	3908	67
0300-0400	4317	68	1500-1600	3830	65
0400-0500	4206	68	1600-1700	3943	66
0500-0600	4222	68	1700-1800	4059	68
0600-0700	4183	69	1800-1900	3973	67
0700-0800	4092	67	1900-2000	3949	67
0800-0900	3983	68	2000-2100	3999	67
0900-1000	4051	69	2100-2200	4050	68
1000-1100	4012	69	2200-2300	4054	67
1100-1200	3952	68	2300-2400	3402	65

Table 4. SC10 Data Base Versus L-Shell

L-Shell	Number of Points	Number of Days
5.0-5.49	3222	25
5.5-5.99	18765	69
6.0-6.49	12811	69
6.5-6.99	13174	69
7.0-7.49	17000	69
7.5-7.99	15357	63
> 8.0	15589	49

Table 5. SC10 Data Base Versus K_p

K_p	Number of Points	Number of Days
0	4037	13
1	16186	28
2	16606	42
3	22714	47
4	18315	41
5	10313	29
6	4149	15
7	2820	12
8	788	3

For the charging statistics, three levels of sunlight charging ϕ_f are used, > 10 V, > 50 V, and > 100 V. (Charging is always negative with respect to the plasma.) The > 10 V level is considered to be a minimum level of charging, the > 50 V level an intermediate level, and the > 100 V a high level, which might create large enough differential charging to cause satellite anomalies. Figures 4-8 are mass plots of ϕ_f versus local time, K_p (times 3), L-shell, magnetic latitude, and R_E respectively. From the plots the following observations can be made: (1) charging is restricted to the period between 1900 LT and 0900 LT even for the lowest 10 V cases; (2) charging > 100 V is not seen for K_p less than 3-, although a case might be made that under the right conditions a K_p of 2+ might be associated with > 100 V charging; and (3) no statistical variations with L-shell, magnetic latitude, or R_E exists over the region sampled by the SCATHA satellite.

The most interesting of the above results, the charging restriction between 1900 and 0900 LT, is more closely examined. Figure 9 is a plot of the percent of days in the sample where charging is > 10 V, > 50 V, and > 100 V. The percentages are given for each 1-hr local time bin. The figure also shows that on 28 days (41 percent of the days sampled) SCATHA charged to over 100 V in sunlight.

Similarly for 38 days (55 percent of the sample days) charging exceeded 50 V and for 47 days (68 percent of the sample days) charging reached at least 10 V. The local time dependence is approximately normally distributed around 0200, the center of the charging interval for all levels. This indicates that the highest probability of encountering an environment conducive to charging at any level occurs around 0200 LT although high level charging can occur anytime during the 1900 - 0900 LT interval. A survey of the SSPM SCATHA data by Mizera and Boyd[4] shows that the probability of Kapton charging to more than 500 V occurs over the same local time interval. It therefore seems that, over the region of space sampled by the SCATHA satellite, only the local time interval between 1900 and 0900 is of interest in looking for a "worst case" charging environment.

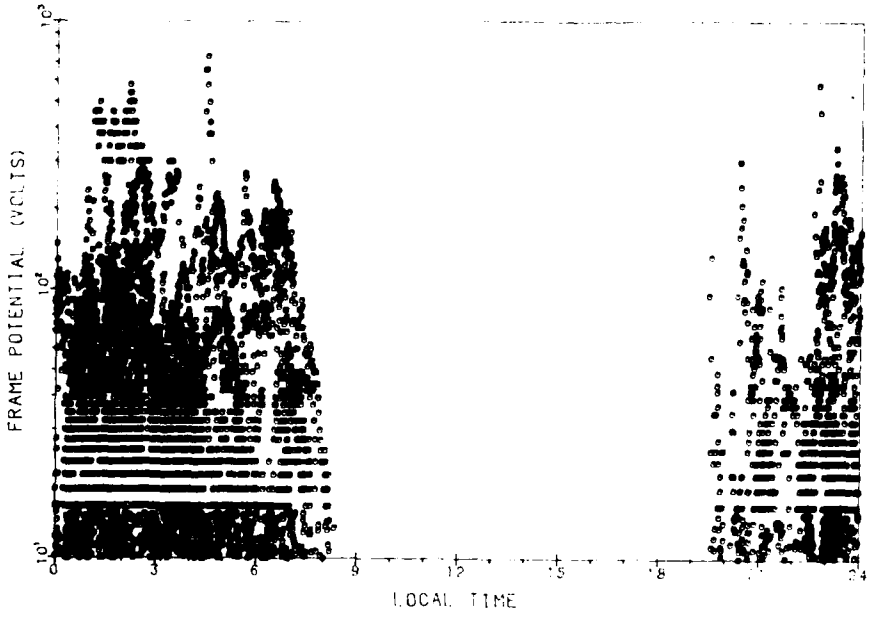

Figure 4. Mass Plot of Frame Potential ϕ_f Versus Local Time for Periods of $\phi_f > 10$ V Negative Over the 69 Day Data Sample Interval. Only the maximum values for each spin period were used

4. Mizera, P. F., and Boyd, G. M. (1982) A Summary of Spacecraft Charging Results, AIAA Reprint 82-0286 presented at the AIAA 20th Aerospace Sciences Meeting, January 11-14, 1982, Orlando, Florida.

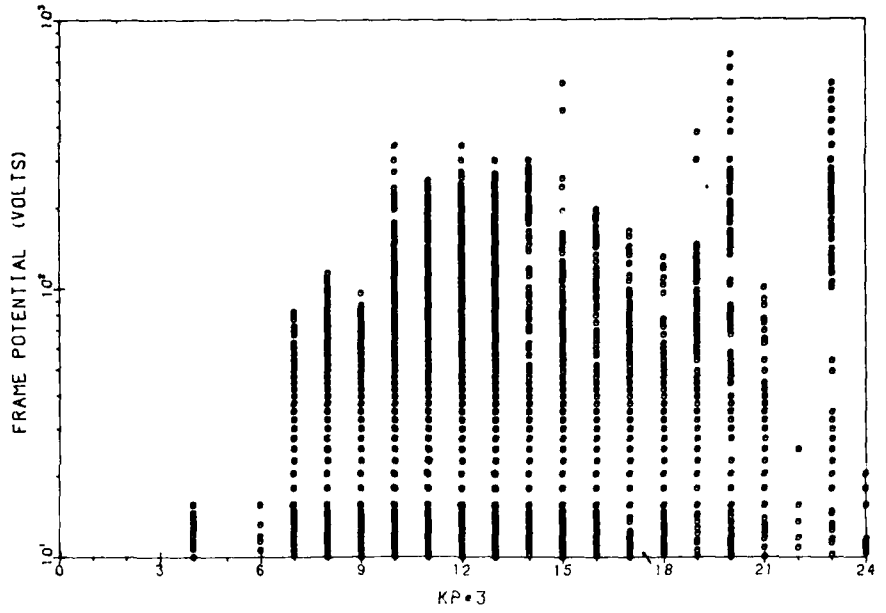

Figure 5. Mass Plot of Frame Potential ϕ_f Versus 3 Times the Magnetic Activity Index K_p. Only the maximum values for each spin period were used

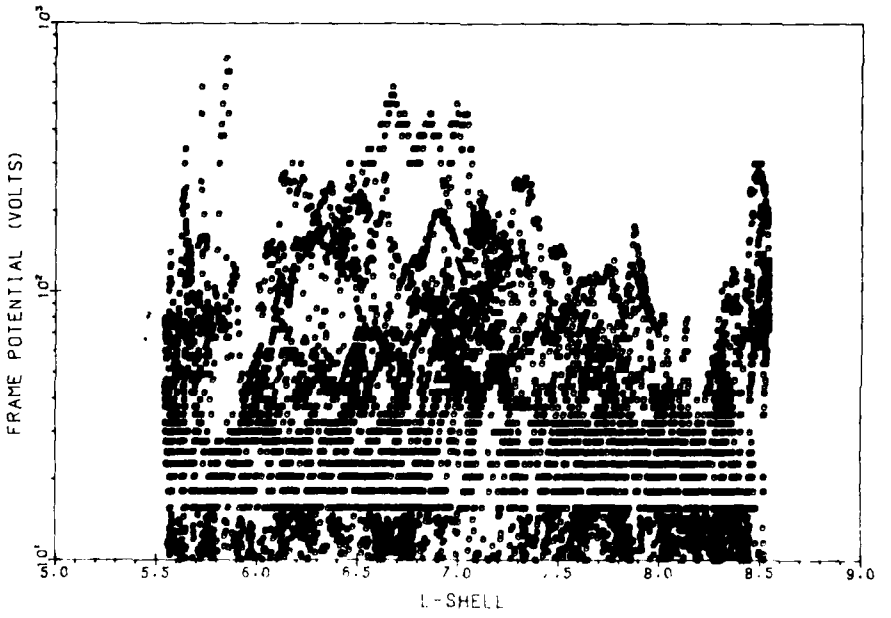

Figure 6. Mass Plot of Frame Potential ϕ_f Versus L-shell. Only the maximum values for each spin period were used

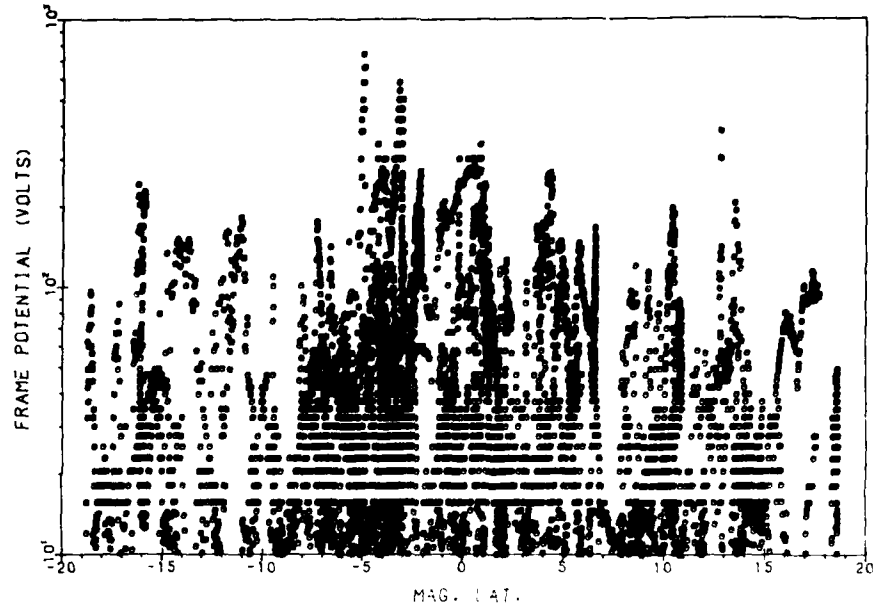

Figure 7. Mass Plot of Frame Potential ϕ_f Versus Magnetic Latitude. Only the maximum values for each spin period were used

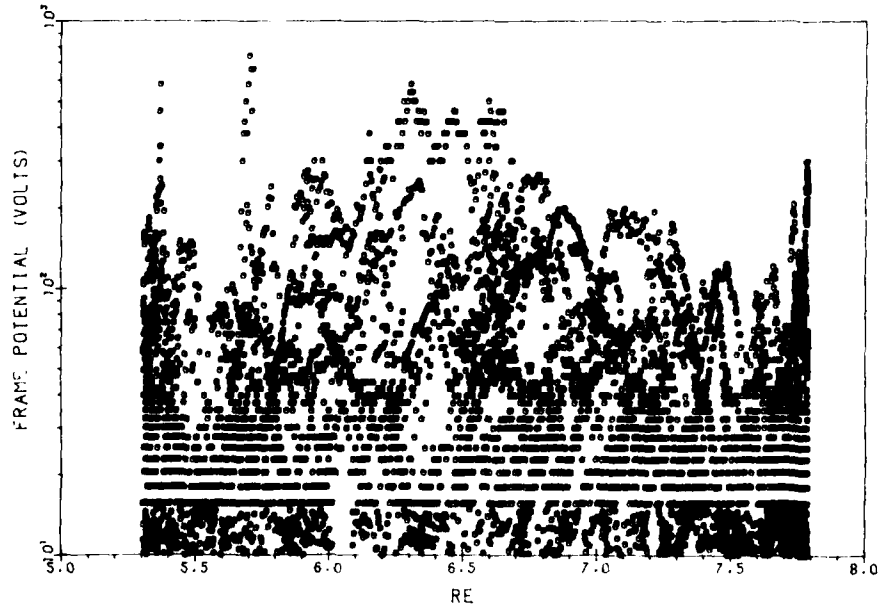

Figure 8. Mass Plot of Frame Potential ϕ_f Versus Altitude in Earth Radii. Only the maximum values for each spin period were used

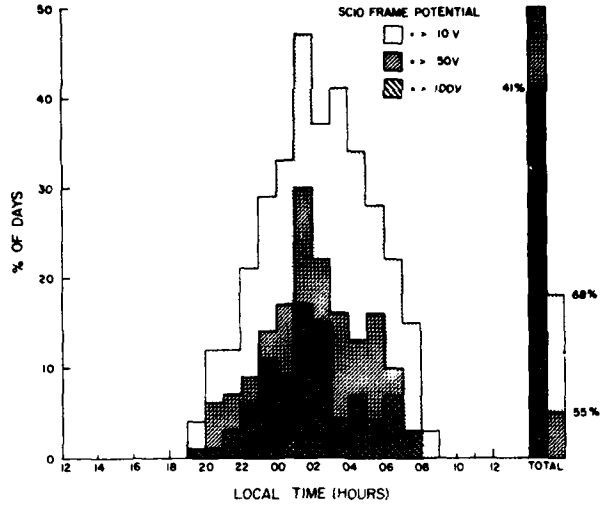

Figure 9. Histogram of the Percentage of Days Frame Potential ϕ_f Reached Values > 10 V Negative, > 50 V Negative, and > 100 V Negative in 1-hr Local Time Bins. Also, the total percentage of days ϕ_f exceeded each level

In Mullen et al[1] a high correlation between the 53 keV electron flux and ϕ_f was shown to exist for the sunlight charging period on day 114, 1979. A survey of all the spin-averaged 53 keV electron flux data for the periods when ϕ_f was greater than 100 V shows that the lowest flux level associated with charging more than 100 V is 6×10^2 elec/cm^2-sec-sr-eV. Using this as a lower level, a full year of SC5 electron data was surveyed (J. Feynman, private communication) to determine when and where the flux level exceeded 6×10^2 elec/cm^2-sec-sr-eV. Results of her study are given in Tables 6 and 7. The number of days SC5 data are available in a particular local time hour bin per R_E bin are given in Table. 6. Table 7 gives the percent of days the 53 keV electron flux is greater than 6×10^2 elec/cm^2-sec-sr-eV in each LT/R_E bin.

The results in Table 7 agree remarkably well with the charging results. Except for two cases between 0900 and 1000 LT, all of the data are between 1900 LT and 0900 LT. Since the low energy plasma environment also controls the charging level, even though a high 53 keV electron flux exists, high level charging may not occur. Figure 10 gives evidence of this. Figure 10 is a mass plot of ϕ_f versus 53 keV electron flux for all the charging values greater than 100 V. It can be seen that for the same flux level, charging can vary over a large range. This is believed to be due to the number of low energy ions available to provide charge balance; the lower the number available, the higher the vehicle charges.

Table 6. SC5 Data Base (Days of data per local time hour per R_E)

Local Time Hour / R_E	12-13	13-14	14-15	15-16	16-17	17-18	18-19	19-20	20-21	21-22	22-23	23-00	00-01	01-02	02-03	03-04	04-05	05-06	06-07	07-08	08-09	09-10	10-11	11-12
5-6	94	101	75	85	76	83	65	70	87	69	87	87	100	105	108	128	113	107	85	62	84	102	95	91
6-7	50	72	69	65	59	62	74	71	57	60	90	100	98	67	62	66	74	65	60	82	65	58	48	37
7-8	108	70	73	84	93	110	103	79	98	96	94	100	99	91	97	78	83	75	70	80	75	74	85	103

Table 7. Percentage of Days on Which the 53.8 keV Electron Flux Exceeded 6×10^2 elec/cm^2-sec-sr-eV

Local Time Hour / R_E	12-13	13-14	14-15	15-16	16-17	17-18	18-19	19-20	20-21	21-22	22-23	23-00	00-01	01-02	02-03	03-04	04-05	05-06	06-07	07-08	08-09	09-10	10-11	11-12
5-6	0	0	0	0	0	0	0	1	2	1	3	12	11	13	12	12	12	15	19	12	5	2	0	0
6-7	0	0	0	0	0	0	0	0	3	3	6	10	14	28	27	27	19	13	15	8	5	0	0	0
7-8	0	0	0	0	0	0	0	0	1	1	0	9	11	12	12	15	14	13	10	7	3	0	0	0

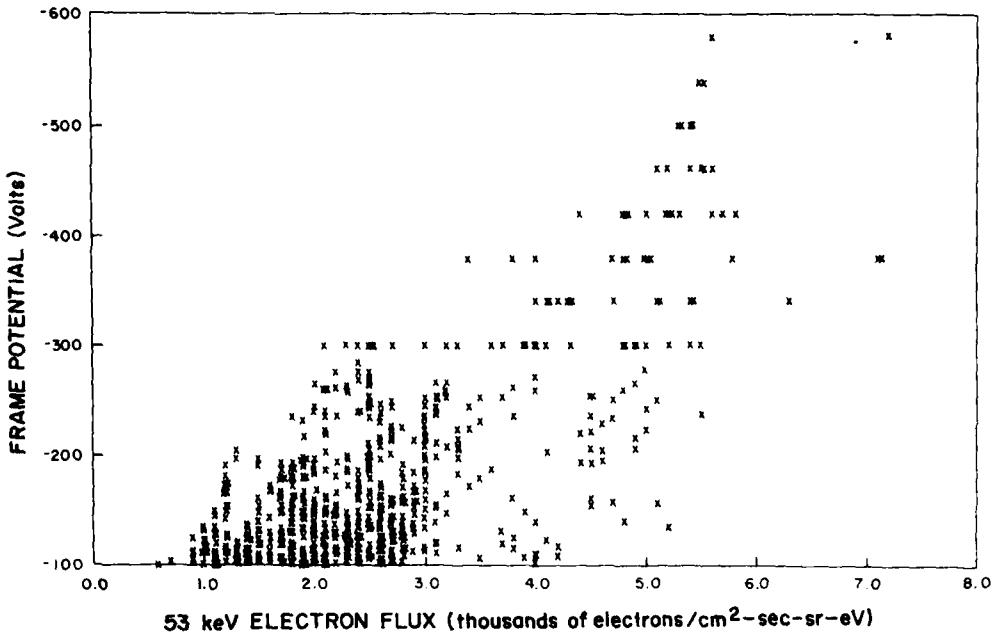

Figure 10. Mass Plot of Frame Potential ϕ_f Versus 53 keV Electron Flux for All Times the Spin Maximum Exceeded 100 V Negative Over the 69-Day Sample Set

In summary, in the geosynchronous region between 5.3 and 7.8 R_E, high level spacecraft charging can occur (1) anywhere between 5.3 and 7.8 R_E, (2) at any magnetic latitude between ± 19°, (3) for any L-shell between 5.5 and 8.5, (4) any time K_p is 2+ or greater, and (5) for any local time between 1900 and 0900 LT. How far outside of the sampled region high level charging can occur cannot be determined since the data are not available. However, anywhere the plasma conditions we discuss as the "worst case" conditions in the next section exist, spacecraft charging can be a problem if proper safeguards are not taken in space vehicle design.

4. *HIGH LEVEL CHARGING ENVIRONMENTS*

Three periods are chosen for study to determine a "worst case" environment for spacecraft charging. The periods are: (1) 0650-0710 UT on day 114, 1979; (2) 1600-1930 UT on day 241, 1979; and (3) 1915-2000 UT on day 363, 1979. In the first period the sunlight charging reached a peak value of -340 V just prior to the largest eclipse charging during the first year of SCATHA operations. In the second,

ϕ_f reached the largest sunlight value measured at the spin peak to date, -740 V at 1921 UT. In the third the maximum value of ϕ_f measured at the spin peak was -580 V, but ϕ_f reached a charging level of -740 V later in the spin (see Figure 3). These periods were also chosen because the charging occurred at different local times. Figure 11 shows the SCATHA orbits (dots) for the three days on which are marked the sunlight charging locations for $\phi_f > 10$ V (thin solid lines) and for $\phi_f > 100$ V (thick solid lines). The eclipse period on day 114 is marked by X's. Table 8 summarizes the orbit parameters.

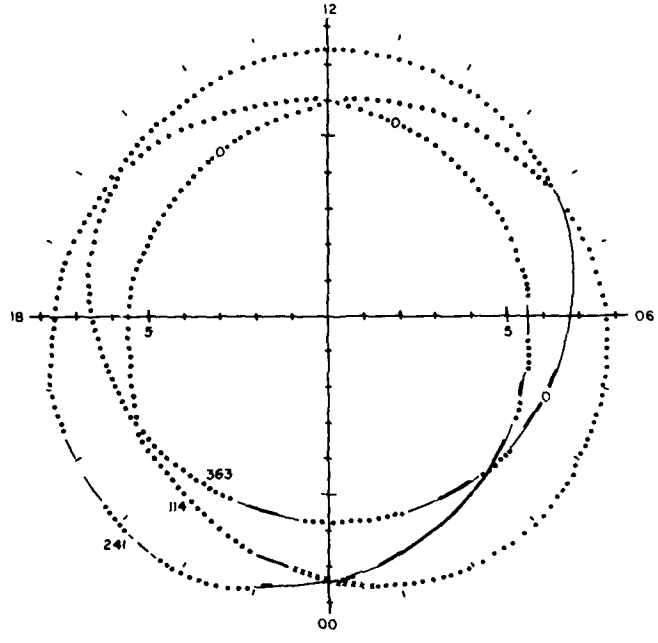

Figure 11. SCATHA Satellite Orbits (dots) in Local Time and L-shell Showing Sunlight Charging Locations and Times When ϕ_f Exceeded 10 V Negative (thin solid lines) and Exceeded 100 V Negative (thick solid lines). The eclipse period on day 114 is shown as x's and the 0000 UT time for each day is shown as a 0

Table 8. SCATHA Time and Position for "Worst Case" Charging Events

Day (1979)	Peak Sunlight Charging Level	LT	L-Shell	K_p	R_E	MLT
114	-340 V	2314	7.1	3+	6.6	2311
241	-740 V	0428	5.8	7-	5.7	0435
363	-580 V	2243	5.7	5	5.4	2230

Figures 12-14 show φ_f versus UT for the three days giving peak charging levels occurring throughout the whole of each day. The scale is linear below 10 V and logarithmic above 10 V. Figures 15-17 show a blowup of the highest level charging peaks for days 114, 241, and 363 respectively, together with a plot of B_z as measured by the SC11 magnetometer on SCATHA over the same period. Superimposed on B_z is the Olson-Pfitzer[5] Field Model. In all three cases the highest charging is coincident with a rapid "snapping back" of the field toward a more dipolar configuration. Ten-minute averages of the particle fluxes (ion and electron) as measured by SC5 between ~300 eV and 400 keV are given in Figures 18-20 for days 114, 241, and 363 respectively. As can be seen in the plots for days 114 and 363, the electron fluxes above 23.8 keV are anisotropic at the time of peak charging. On day 241 the ESA's were off during the peak charging period; however, the 96 keV electron fluxes are nearly isotropic at the charging peak, unlike days 114 and 363. Also on day 241, at approximately 1726 UT, when there was a charging peak of -580 V (see Figure 13), the electron fluxes were isotropic down to the lowest energies.

5. CORRELATION ANALYSIS

In the previous section evidence was presented which indicates that high level charging environments occur during the injection of high energy (> ~20 keV) electrons while the magnetic field is "snapping back" toward a more dipolar configuration. In this section a statistical analysis shows the relationship that exists between φ_f and the electron fluxes.

5. Olson, W.P., and Pfitzer, K.A. (1974) A quantitative model of the magnetospheric field, JGR, 79:3739-3748.

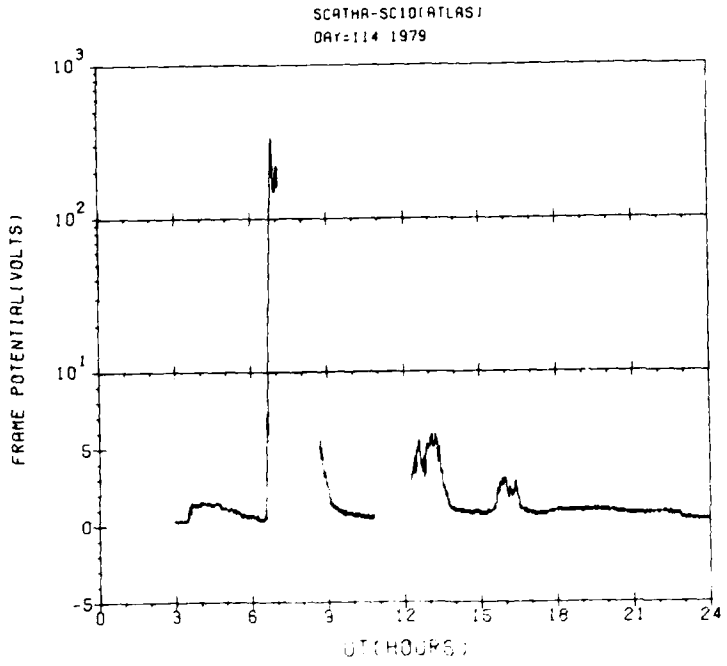

Figure 12. Frame Potential φ_f Versus UT for Day 114, 1979. φ_f represents the spin maximum and is plotted linearly for values less than 10 V (negative) and logarithmically for values greater than 10 V (negative)

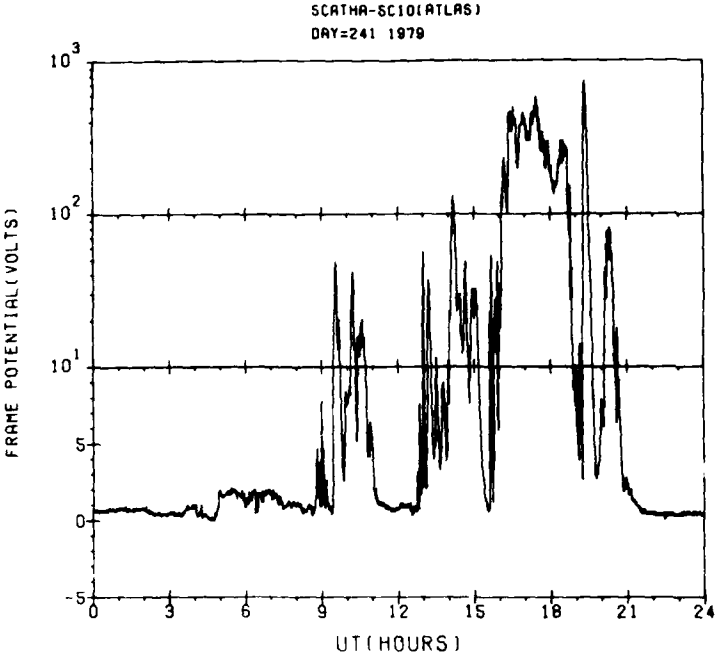

Figure 13. Frame Potential φ_f Versus UT for Day 241, 1979. φ_f represents the spin maximum and is plotted linearly for values less than 10 V (negative) and logarithmically for values greater than 10 V (negative)

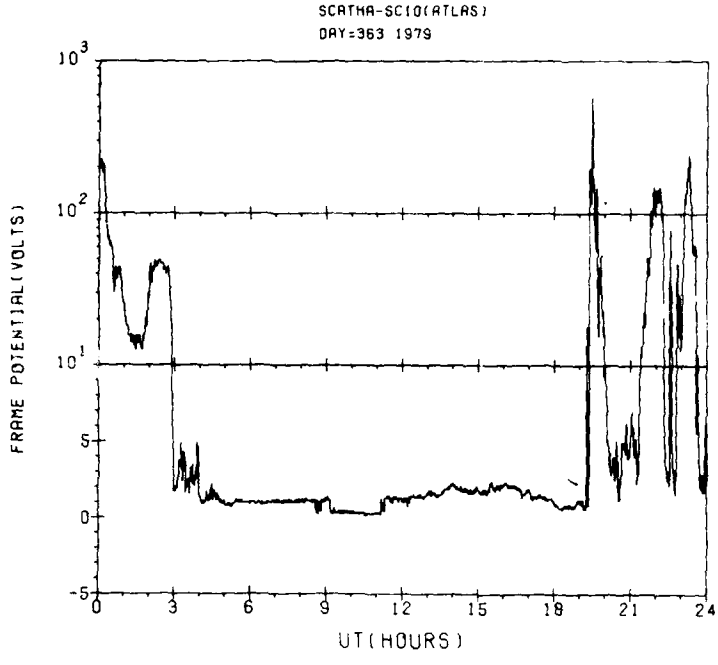

Figure 14. Frame Potential φ_f Versus UT for Day 363, 1979. φ_f represents the spin maximum and is plotted linearly for values less than 10 V (negative) and logarithmically for values greater than 10 V (negative)

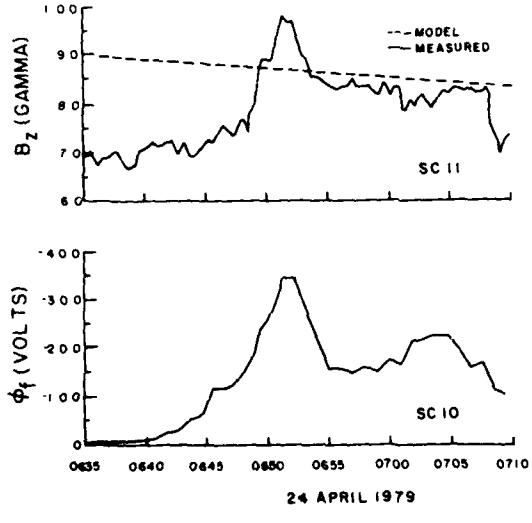

Figure 15. A Time History of Vehicle Frame Charging Between 0635 and 0710 UT on Day 114, 1979, Together With the Associated B_z Component of the Magnetic Field. The top panel shows the B_z component of the magnetic field in Solar Magnetic coordinates as measured by SC11 (solid line) and the Olson and Pfitzer quiet model for the same interval (dashed line). The bottom panel shows φ_f as measured through the peak charging period

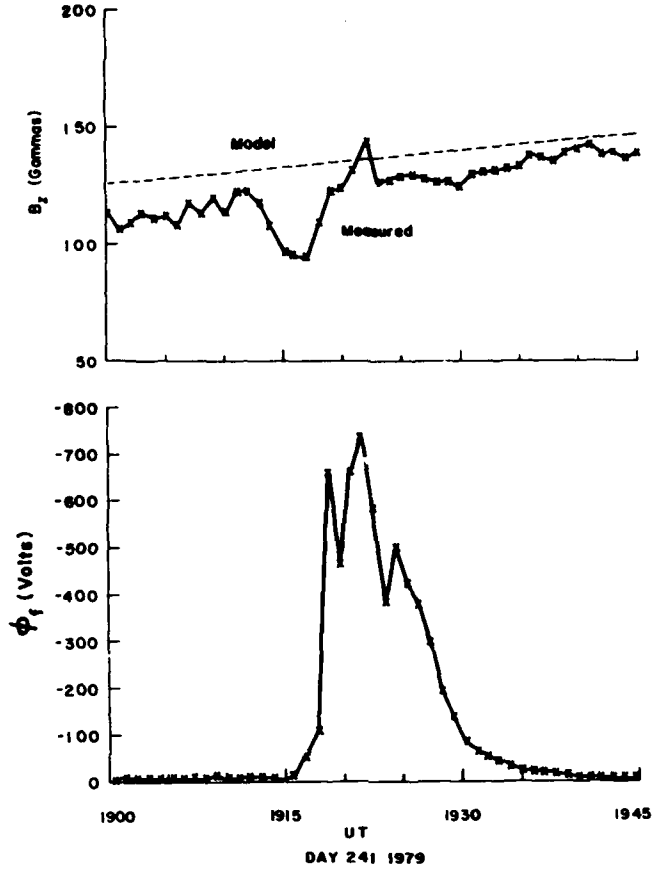

Figure 16. A Time History of Vehicle Frame Charging Between 1900 and 1945 UT on Day 241, 1979 Together With the Associated B_z Component of the Magnetic Field. The top panel shows the B_z component of the magnetic field in Solar Magnetic coordinates as measured by SC11 (solid line) and the Olson and Pfitzer quiet model for the same interval (dashed line). The bottom panel shows frame potential ϕ_f as measured through the peak charging period

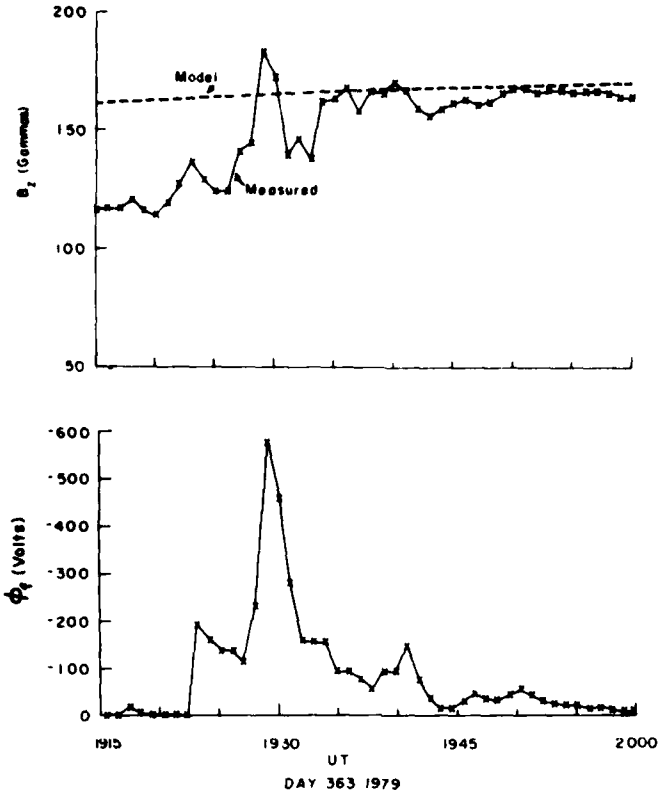

Figure 17. A Time History of Vehicle Frame Charging Between 1915 and 2000 UT on Day 363, 1979 Together With the Associated B_Z Component of the Magnetic Field. The top panel shows the B_Z component of the magnetic field in Solar Magnetic coordinates as measured by SC11 (solid line) and the Olson and Pfitzer quiet model for the same interval (dashed line). The bottom panel shows frame potential ϕ_f as measured through the peak charging period

To make a quantitative assessment of the relationship between electron fluxes and ϕ_f, linear regressions between the two are performed for each energy channel from 0.62 keV to 335 keV during sunlight charging periods. On day 114 the regressions are performed for the period 0635-0710 UT, and on day 363 for the period 1922-2000 UT. On day 241, the regressions are performed over two intervals before and after the maximum charging period, from 1650-1755 UT and from 1954-2041 UT respectively, since data below 96 keV do not exist for the maximum charging period. The data are from periods when the detector was sampling ~90° to the magnetic field, the direction of maximum flux. The correlation coefficients (r) are given in Table 9.

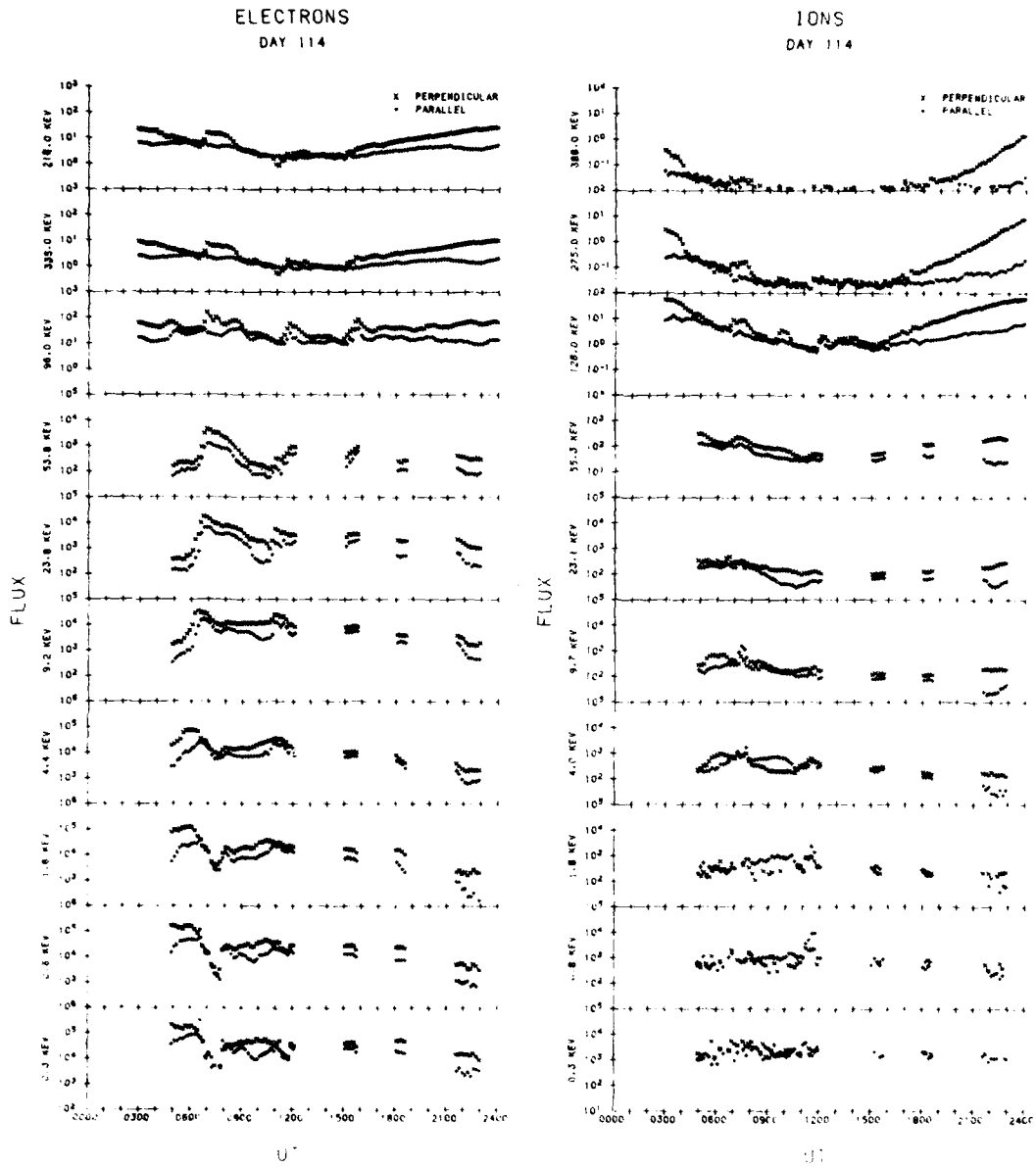

Figure 18. Ten-minute Averages of SC5 Electron (left) and Ion (right) Fluxes in Particles-cm^{-2}-s^{-1}-sr^{-1}-eV^{-1} as Measured Perpendicular (x's) and Between 150° and 175° (plus signs) to the Magnetic Field for Energy Channels Between 0.3 and 400 keV Versus UT on Day 114, 1979

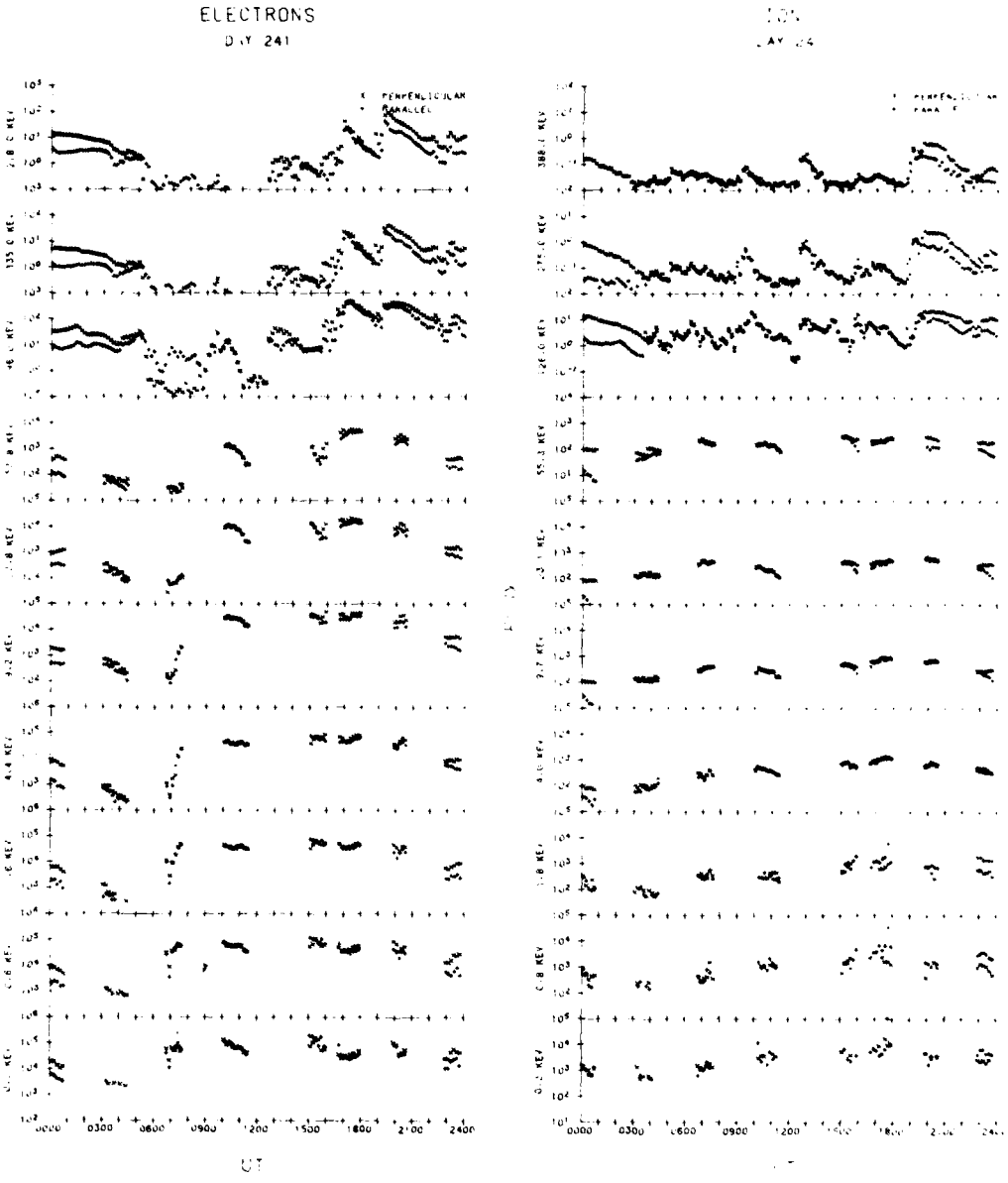

Figure 19. Ten-minute Averages of SC5 Electron (left) and Ion (right) Fluxes in Particles-cm^{-2}-s^{-1}-sr^{-1}-eV^{-1} as Measured Perpendicular (x's) and Between 150° and 175° (plus signs) to the Magnetic Field for Energy Channels Between 0.3 and 400 keV Versus UT on Day 241, 1979

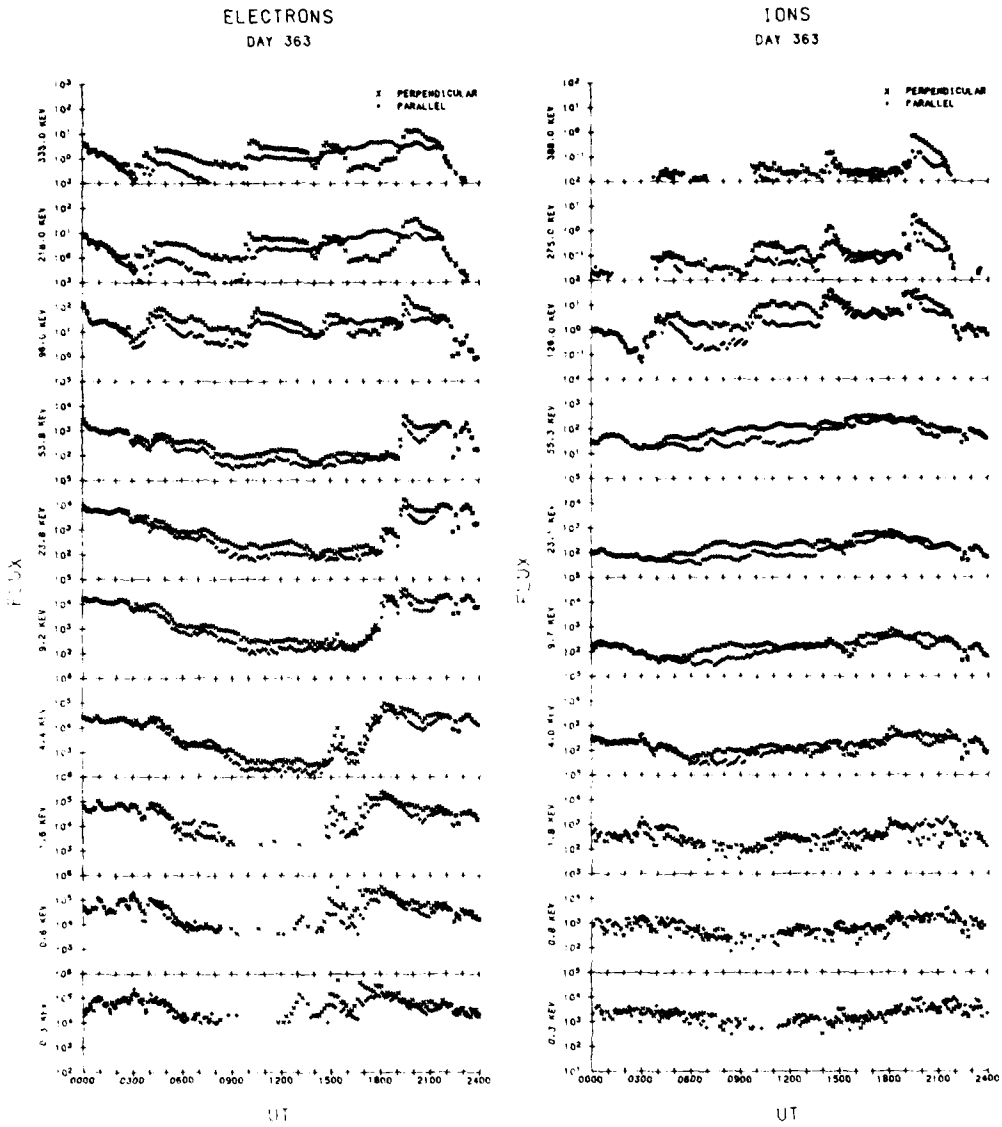

Figure 20. Ten-minute Averages of SC5 Electron (left) and Ion (right) Fluxes in Particles-cm^{-2}-s^{-1}-sr^{-1}-eV^{-1} as Measured Perpendicular (x's) and Between 150° and 175° (plus signs) to the Magnetic Field for Energy Channels Between 0.3 and 400 keV Versus UT on Day 363, 1979

Table 9. Correlation Coefficients of Frame Potential ϕ_f Versus Electron Flux

SC5 Energy Bin (keV)	Day 114 (37 Points)	Day 241 (114 Points)	Day 363 (41 Points)
0.62	-0.87	-0.10	-0.48
1.57	-0.72	+0.08	-0.28
4.4	-0.28	+0.25	+0.21
9.2	-0.36	+0.50	+0.58
23.8	+0.42	+0.83	+0.75
53.8	+0.94	+0.87	+0.87
96	+0.85	+0.01	+0.63
218	+0.92	-0.46	+0.38
335	+0.92	-0.28	+0.58

Two things are evident from the table. The first is that the 53.8 keV electron flux always has the highest correlation with ϕ_f. The second is that the total energy range that correlates with charging can shift depending on the total ambient plasma environment and its relative distribution of particles. The second point is discussed in more detail later in the report. The reason that the 53.8 keV electron flux has the highest correlation with sunlight charging is not clear. It might be due to the fact that the 53.8 keV flux best represents the energy distribution range most causative to charging, or it might be due to the 53.8 keV electron flux channel producing the most net charging current to the satellite after all effects to include backscattered particles, secondaries, and so on, are considered. Whatever the reason, the electron energy range most closely correlated with ϕ_f is the energy range of the 53.8 keV electron channel, ~30 keV to ~75 keV. If one desires an instrument that looks for a ϕ_f charging environment, a detector measuring electron flux over this energy range would be ideal. The only parameter then missing to determine the charging level from the flux would be the low energy plasma environment which provides the current balance. However, once a certain high level electron flux environment was encountered a flag could indicate that large charging was possible. Again, the charging level would depend on satellite design, configuration and material and the low energy plasma environment.

6. MOMENTS OF THE DISTRIBUTION FUNCTION

Certain properties of the plasma can be calculated by taking various velocity moments of the ion and electron distribution functions constructed from particle measurements. For SC5, the first four moments (zero-order through third-order) are related to number densities and fluxes of a given particle species as follows:

Number density, n:		$\int f\, d^3v \ (cm^{-3})$,	(1)
Number flux, NF:		$\int \lvert v \rvert f\, d^3v \ (cm^{-2}\text{-}s^{-1})$,	(2)
Energy density, ϵ:	1/2 m	$\int v^2 f\, d^3v \ (eV\text{-}cm^{-3})$,	(3)
Energy flux, EF:	1/2 m	$\int \lvert v^3 \rvert f\, d^3v \ (eV\text{-}cm^{-2}\text{-}s^{-1})$.	(4)

In these equations, f and m are the distribution function and mass for a given particle species, and the integration is taken over the entire velocity space. For the SC5 measurements, symmetry is assumed in the plasma perpendicular to the magnetic field and integrations are performed over pitch angle and velocity. The fluxes (number and energy) in Eqs. (2) and (4) are the total fluxes that would be intercepted by an infinitesimally small, omni-directional receiving device. In practice directional fluxes ($cm^{-2}\text{-}s^{-1}\text{-}sr^{-1}$) are often used (no integration in angular space). In order to incorporate pitch angle information, average directional fluxes can be calculated from Eqs. (2) and (4) by dividing by 4π.

From the first four moments there are two ways of defining temperature:

$$(1) \quad T_{AVG} = \frac{2}{3} \cdot \frac{\epsilon}{n}, \tag{5}$$

and

$$(2) \quad T_{RMS} = \frac{1}{2} \cdot \frac{EF}{NF}. \tag{6}$$

For a distribution function that is well fit by the Maxwell-Boltzmann function,

$$f(v) = n \left(\frac{m}{2\pi kT} \right)^{3/2} e^{-mv^2/2kT}, \tag{7}$$

the two temperatures are equal; that is,

$$T = T_{RMS} = T_{AVE}. \tag{8}$$

[In Eq. (7), k is the Boltzmann constant = 1.38×10^{-16} erg/°K.] In general, however, distribution functions are not Maxwellian over the entire energy range and the concept of temperature is an ambiguous one.

Table 10 gives the first four moments of the ion and electron distribution functions, together with T_{AVE} and T_{RMS} for times near the peak charging level on

each day. The SC5 measurements over the energy range 100 eV - 400 keV are used to construct the distribution functions (the total distribution for the SC5 instrument). Integrations over pitch angle are used for all moments. The moments for ions are calculated assuming hydrogen as the only species. The moments are calculated for day 114 at 0651 UT at a ϕ_f of -340 V; for day 241 at 1726 UT at a ϕ_f of -580 V; and for day 363 at 1929 UT at a ϕ_f of -580 V. Care must be taken in interpreting the moment results since the cold population is missing and the low energy end of the spectrum is influenced by ϕ_f.

Table 10. Moments and Temperatures Integrated Over Pitch Angle (100 eV - 400 keV)

	Electrons			Ions			
Day	114	241	363	114	241	363	Units
n	0.74	2.6	2.0	2.3	4.0	2.2	cm^{-3}
NF	4.3×10^{9}	1.3×10^{10}	1.0×10^{10}	1.8×10^{8}	4.0×10^{8}	2.4×10^{8}	$cm^{-2}-s^{-1}$
ED	9.2×10^{3}	2.4×10^{4}	2.0×10^{4}	1.5×10^{4}	3.7×10^{4}	2.8×10^{4}	$eV-cm^{-3}$
EF	8.4×10^{13}	1.9×10^{14}	1.8×10^{14}	4.0×10^{12}	9.4×10^{12}	1.1×10^{13}	$eV-cm^{-2}-s^{-1}$
T_{AVE}	8.4	6.2	6.8	4.3	6.1	8.8	keV
T_{RMS}	9.8	7.6	8.7	11.1	11.7	22.6	keV

Table 11 gives the moments and temperatures over the energy range 20 - 400 keV (called the high energy moments) for the same time periods. Tables 10 and 11 together show very little difference between day 241 and day 363 electron moments. Day 114, however, gives lower values for all the moments. Recall that the charging on day 114 was significantly lower than the other two days. If on day 241 the electron density (20 - 400 keV) is extrapolated to the appropriate values for ϕ_f = -740 V using a linear regression analysis with a correlation coefficient of 0.94, the density is 0.64 electrons/cm^3. This is approximately 25 percent higher than the value measured at -580 V and given in Table 11.

How well the electron moments correlate with $\phi_f > 10$ V is shown in Table 12. The high energy moments significantly correlate with ϕ_f with nearly the same r's. This is because the temperature remains nearly constant over the time interval of charging. Also the highest total moment, EF(T), correlates at nearly the same level as the high moments. This is because higher moments are weighted toward

higher energies (Eqs. 1-4). The differences in the absolute value of r among the three days may result from variations in the low energy plasma environment over the sample period; the greater the variation in the low energy plasma, the lower the expected r.

Table 11. Moments and Temperatures Integrated Over Pitch Angle (20 - 400 keV)

	Electrons			Ions			
Day	114	241	363	114	241	363	Units
n	0.24	0.51	0.48	0.26	0.79	0.48	cm^{-3}
NF	2.4×10^{9}	4.9×10^{9}	4.7×10^{9}	7.2×10^{7}	2.0×10^{8}	1.4×10^{8}	$cm^{-2}\text{-}s^{-1}$
ED	6.7×10^{3}	1.4×10^{4}	1.4×10^{4}	1.1×10^{4}	2.8×10^{4}	2.4×10^{4}	$eV\text{-}cm^{-3}$
EF	7.1×10^{13}	1.5×10^{14}	1.5×10^{14}	3.6×10^{12}	8.3×10^{12}	1.0×10^{13}	$eV\text{-}cm^{-2}\text{-}s^{-1}$
T_{AVE}	18.6	18.4	18.6	27.1	23.4	33.6	keV
T_{RMS}	15.2	15.1	15.3	24.9	20.6	36.0	keV

Table 12. Correlation Coefficients of Frame Potential ϕ_f Versus Electron Moments

Moment*	Day 114 (Number of Points)	r	Day 241 (Number of Points)	r	Day 363 (Number of Points)	r
n (H)	58	0.85	159	0.94	321	0.69
NF (H)	58	0.87	159	0.94	321	0.70
ED (H)	58	0.90	159	0.94	321	0.71
EF (H)	58	0.91	159	0.94	321	0.71
n (T)	58	0.17	159	0.47	321	0.21
NF (T)	58	0.64	159	0.78	321	0.52
ED (T)	58	0.78	159	0.90	321	0.64
EF (T)	58	0.86	159	0.94	321	0.69

*H = high = 20 keV - 400 keV; T = total = 100 eV - 400 keV

Given the high correlation of the electron moments with ϕ_f, we feel that these are the best parameters to use to specify the high level charging environment. However, we are also aware of the desires of certain modelers and designers in the engineering community to have distribution functions and simplified representations of these distribution functions. The next section will address this area.

7. DISTRIBUTION FUNCTIONS

We have found that at times of substantial sunlight charging (> 100 V) the SCATHA satellite encounters high fluxes of electrons with energies greater than 20 keV, in the absence of a cold ion population. Although good measurements of the high energy plasma characteristics are obtained on SCATHA, a detailed understanding of how current balance is achieved is hampered by lack of: (1) measurement of the cold plasma population, (2) high resolution measurements of particles along the magnetic field, (3) an understanding of the extent to which the cold population is trapped in the vicinity of the satellite and possibly reflected back to the satellite, and (4) the dependence of backscattered and secondary electrons on the primary spectrum.

Thus, it is insufficient to specify only the moments of the measured high energy particle distributions, even though they directly relate to the currents that drive the satellite potential. The contribution that can be made from the particle measurements on SCATHA is the specification of the distribution of the high energy population during charging. In this section the actual distribution functions for peak levels of charging on days 114, 241, and 363 are presented. The problems that arise in fitting these distributions by a double Maxwellian are discussed. A method of fitting the distributions is determined which best maintains the essential characteristics of the high energy plasma during charging.

Figures 21a, 21b, and 21c show electron distributions from days 114, 241, and 363, respectively. The distribution functions are for measurements perpendicular to the magnetic field. We use these distribution functions with the assumption of isotropy to represent the plasma. A measure of the anisotropy of the plasma can be taken from Figures 18-20. Using the perpendicular distribution function with the assumption of isotropy will lead to an overestimation of plasma parameters, such as the moments, for charging periods. Recall that the assumption of isotropy is a particularly good one for day 241. In Figure 21 the distributions shown by dashed lines are from the nearest pre-charging period available. The solid lines show the distributions for the peak charging periods. The following observations can be made concerning the distributions: (1) The three sets of distribution functions are remarkably similar. The pre-charging distributions for both ions and electrons have

a distinct "knee" at ~10 keV for electrons and ~100 keV for ions. On either side of the knee the variation of the distribution with energy behaves as a power law (linear on a log-log plot). (2) The peak charging distributions vary from the pre-charging distributions in the same way on all three days, with an increase on the high side of the knee and a depletion on the low side. The high energy electrons appear to be somewhat heated in the process. (This does not contradict the assertion that during charging the temperature variations are of secondary importance to the density variations.) (3) The lowest energy channels (less than the satellite potential) do not show consistent variations. On day 114 the ion fluxes less than 1 keV were below detectability pre-charging, and showed no enhancement during charging. On day 363 the same pre-charging ion flux levels fell below detectability during charging. On day 241 the satellite potential apparently enhances the low energy ion flux to the vehicle. The lowest energy electron fluxes are depressed on two of the days during charging, 241 and 363, and unaffected on the third, 114. These different low energy particle behaviors indicate either variations in the low energy ambient plasma, or various forms of low energy access to the satellite perpendicular to the magnetic field, or a combination of the two.

Greater spectral detail of the electron distributions in the energy range 4-400 keV is given in Figure 22. Here the peak charging distributions for the three days are plotted one on top of the other, on a log-linear scale. Again, the similarity of the high energy environments for all three days is remarkable. In addition, it is quite clear that the distributions are not Maxwellian throughout the entire energy range. A Maxwellian distribution on a log-linear scale is a straight line. Instead, the slopes of these three distributions continuously decrease with increasing energy. We have agreed, for analytic simplicity, to represent the charging environment by at most four parameters, n_1 n_2, T_1, T_2, which can be used to construct a two-Maxwellian distribution (refer to Mullen et al[1]). It is clear from Figure 22 that this is not a particularly good representation for the high energy range. Figure 21 indicates that the choice of a Maxwellian distribution will probably also be poor for low energies. Nevertheless, we can make use of a certain amount of latitude in choosing the portion of the high energy distribution we fit to the Maxwellian in order to insure that the major features of the charging environment are well-represented, or are at least over—rather than underestimated. Briefly these include: (1) emphasis on changes in fluxes between 20 keV and 100 keV; (2) high correlation of charging with the number density, number flux, and energy flux calculated over this energy range; and (3) low correlation with "temperature" changes (temperature over the high energy range is defined as being proportional to the ratio of the energy flux to the number flux over the energy range considered).

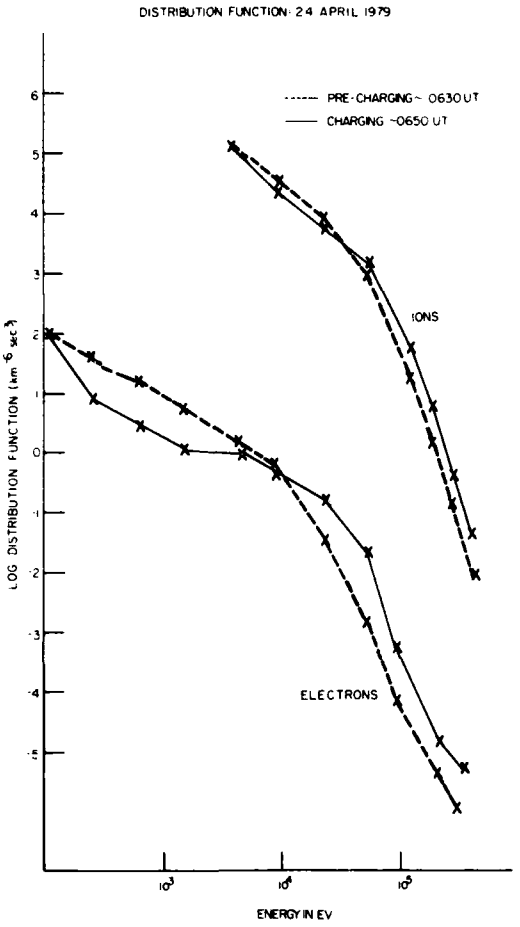

Figure 21a. Distribution Functions of Ions and Electrons Measured Perpendicular to the Magnetic Field Prior to Charging (dashed line) and During the Peak Charging Levels (solid lines) on Day 114, 1979

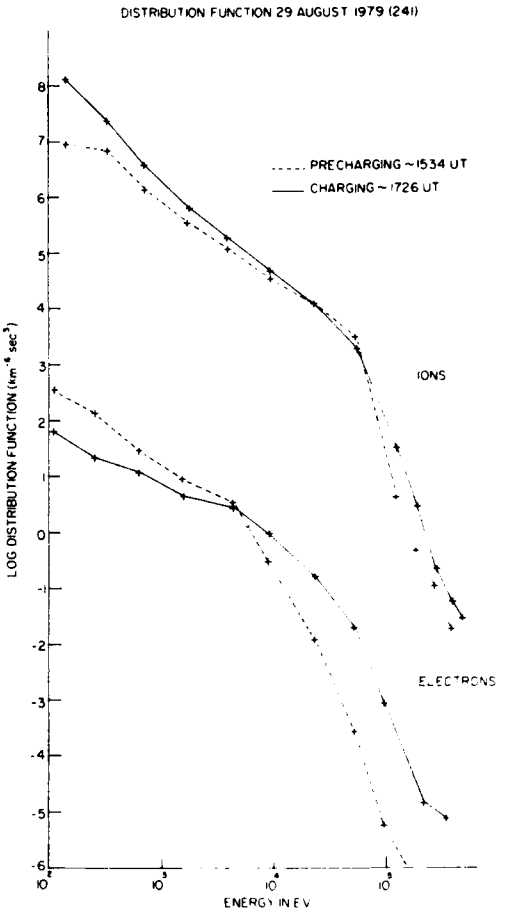

Figure 21b. Distribution Functions of Ions and Electrons Measured Perpendicular to the Magnetic Field Prior to Charging (dashed line) and During the Peak Charging Levels (solid lines) on Day 241, 1979

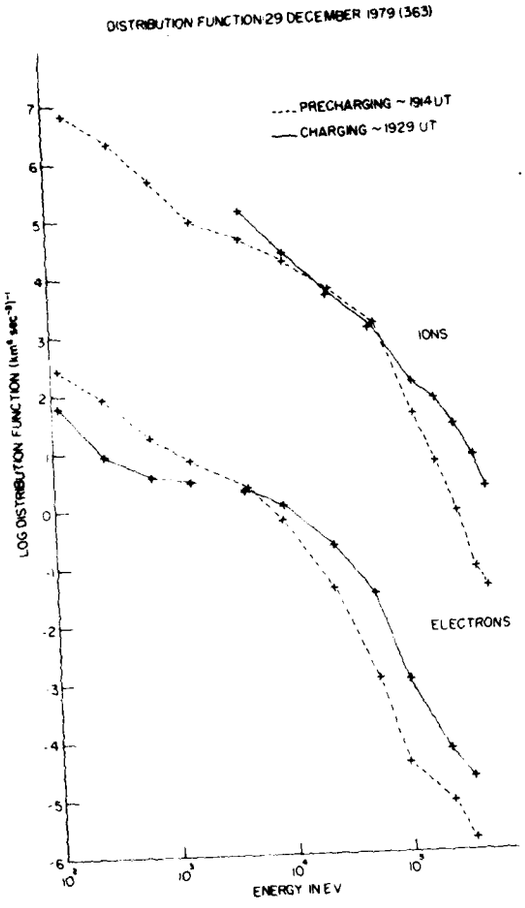

Figure 21c. Distribution Functions of Ions and Electrons Measured Perpendicular to the Magnetic Field Prior to Charging (dashed line) and During the Peak Charging Levels (solid lines) on Day 363, 1979

The measured values of the electron distribution function for day 241 at the peak level of charging are again shown in Figure 23 (triangles). In addition, the results of linear regressions performed for various energy ranges are shown with their resulting Maxwellian temperatures and densities.

Two obvious choices for the low energy cut-off are 4 keV, where the knee in the distribution occurs (see Figure 21b); and 20 keV, which is the lowest energy channel that correlates highly with satellite frame potential. The high energy cut-offs are taken as either 400 keV, the full range; or 100 keV, the highest energy that makes a significant contribution to the number flux in all three cases discussed.

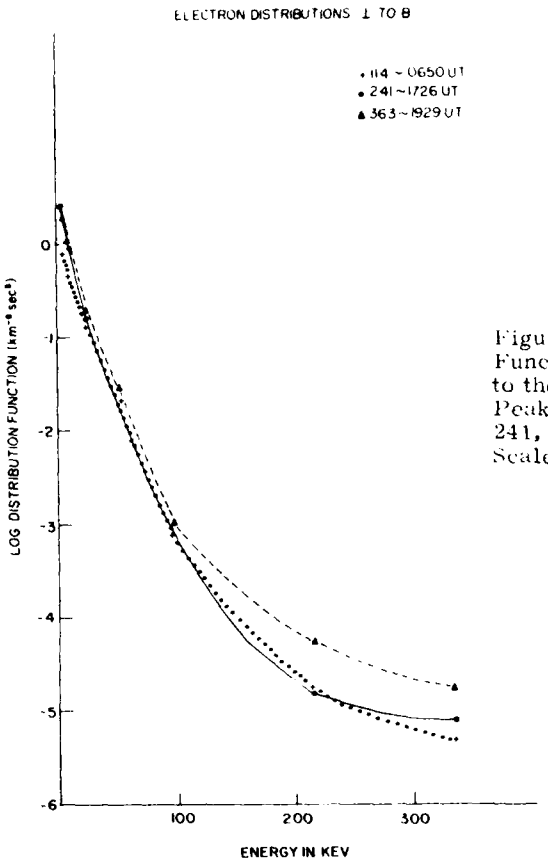

Figure 22. Electron Distribution Functions Measured Perpendicular to the Magnetic Field During the Peak Charging Levels on Days 114, 241, and 363 Using a Linear Energy Scale

The densities and temperatures resulting from the four linear regressions are given in Table 13. Depending on energy range the temperature can vary by a factor of 3 and the density by a factor of 6.

The choice of the range from 20-100 keV uses only three points to calculate the straight line fit. The parameters that result (14 keV, 1.6 cm^{-3}), including the number and energy fluxes (not given), are in good agreement with the high energy moments discussed in previous sections. Expanding this range to include the highest energies (20-400 keV) radically shifts the temperature and the density in opposite directions (32 keV, 0.5 cm^{-3}) to accommodate the high energy tail, and thus, this Maxwellian is a very poor fit in the energy range of importance to charging.

Using the energy range weighted to the lower end, from 4 to 100 keV gives a temperature and density of 12 keV and 3.1 cm^{-3}, respectively. Here the number density is excessive, much of it resulting from the 4-10 keV range which is

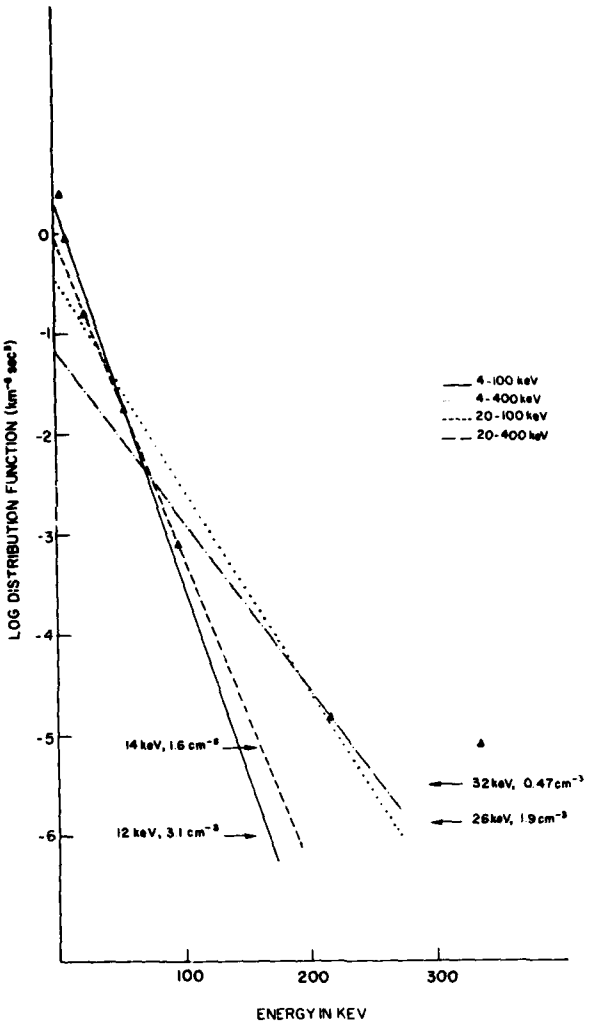

Figure 23. Linear Fits to the Peak Charging Electron Distribution Function on Day 241 Using Various Energy Ranges

unrelated, for the most part, to charging levels. Therefore, variation in this range can greatly affect variations in n_2 without relating to charging. Finally, the full range 4-400 keV gives a temperature and density of 26 keV and 1.9 cm^{-3}, respectively. Here the density is approximately that found from the high energy moments, but the temperature is overestimated by a factor of 2, leading to overestimates of the number and energy fluxes. This linear fit gives good agreement in the range of 20 keV and in the range of 200 keV. It overestimates contributions from the 53 and 96 keV channels, and underestimates the contribution from the 335 keV channel.

Table 13. Linear Regression Densities and Temperatures Versus Energy

Energy Range (keV)	n (cm^{-3})	T (keV)
4-100	3.1	12
4-400	1.9	26
20-100	1.6	14
20-400	0.5	32

While the first range discussed (20-100 keV) gives the closest approximation to the high energy moments for this case, there may be events for which the fluxes greater than 100 keV are significant (see, for example, correlations on day 114). Thus, as a general method for determining the worst case environment Maxwellian representation, we use instead, the entire high energy range from 4-400 keV as the next best, but safer choice. This range was used to calculate the high energy Maxwellian in Mullen et al[1] and was found to represent well those variations which best correlated with the satellite frame potential.

8. TWO-MAXWELLIAN DESCRIPTION OF THE ENVIRONMENT

As is shown above, a two-Maxwellian does not fit the environment during high level charging periods and the method used to fit the data will determine the absolute values of the densities and temperatures. However, relative behavior of the densities and temperatures can be seen in the two-Maxwellian parameters if a consistent method is used. The method used below is the same least-squares fit method as used by Mullen et al[1] over the energy range 4-400 keV for the high component. This method was chosen for reasons discussed there and above: namely they underestimate the lower energy spectrum (below 10 keV) and they overestimate the spectrum in the energy range 20-200 keV shown to be most directly causative of charging. This ensures some safety margin in defining a "worst case".

Figures 24-26 show the two-Maxwellian electron parameters n_1, n_2, T_1, and T_2 for the high level charging periods on days 114, 241, and 363 respectively. On all three days the high Maxwellian temperature T_2 is seen to be nearly constant through the charging peak while the high electron density n_2 peaks at the charging peak in all cases. The low energy temperatures T_1 and densities n_1 vary considerably, but in all cases, n_1 is less than n_2 at the charging peak. (Caution is advised in using the low energy values.) Table 14 gives the "worst case" least-squares

particle environment fits for the charging peaks on days 114, 241, and 363. The highest electron n_2's are on day 241, and therefore, 241, since it did also have the highest sunlight charging peak, will be used as the "worst case."

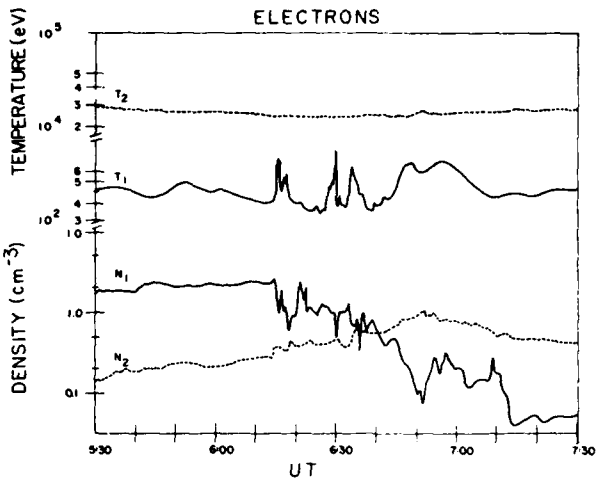

Figure 24. Two-Maxwellian Electron Temperatures T_1 and T_2 and Densities n_1 and n_2, Calculated by Least-Squares Fitting the Distribution Functions Perpendicular to the Magnetic Field Between 4 and 400 keV, Plotted Versus UT for the Time Period From 0530 to 0730 UT on Day 114, 1979

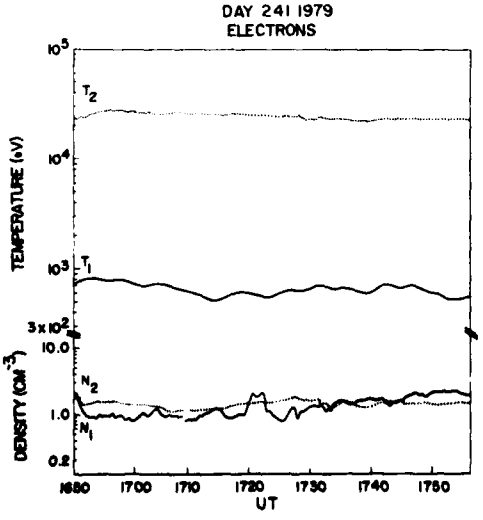

Figure 25. Two-Maxwellian Electron Temperatures T_1 and T_2 and Densities n_1 and n_2, Calculated by Least-Squares Fitting the Distribution Functions Perpendicular to the Magnetic Field Between 4 and 400 keV, Plotted Versus UT for the Time Period From 1650 to 1755 UT on Day 241, 1979

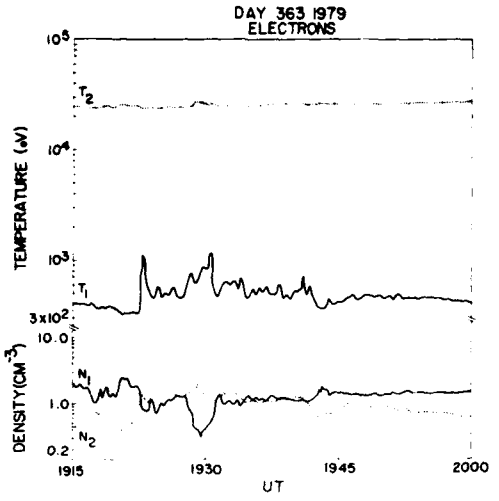

Figure 26. Two-Maxwellian Electron Temperatures T_1 and T_2 and Densities n_1 and n_2, Calculated by Least-Squares Fitting the Distribution Functions Perpendicular to the Magnetic Field Between 4 and 400 keV, Plotted Versus UT for the Time Period From 1915 to 2000 UT on Day 363, 1979

Table 14. Least-Squares Fits of the Particle Environments at the Charging Peaks

			Ions				Electrons			
Day	UT	Mag Field Orientation	n_1 (cm^{-3})	n_2 (cm^{-3})	T_1 (keV)	T_2 (keV)	n_1 (cm^{-3})	n_2 (cm^{-3})	T_1 (keV)	T_2 (keV)
114	~0651	⊥	0.6	1.2	0.2	28.0	0.2	1.2	0.4	27.5
		∥	1.5	0.6	0.5	24.7	0.1	0.3	0.5	25.8
241	~1726	⊥	0.9	1.6	0.3	25.6	0.8	1.9	0.6	26.1
		∥	1.1	1.7	0.4	24.7	1.0	1.5	0.6	25.1
363	~1929	⊥	1.7	1.2	0.2	41.7	0.6	1.8	0.6	29.3
		∥	1.4	1.3	0.4	34.2	1.2	0.8	0.5	24.8

9. CONCLUSIONS

To determine a "worst case" environment and the region of applicability, many of the problems associated with such a study have been discussed. Since the data sets are limited and the particle distributions are not well represented by two-Maxwellians but need to be represented by some limited set of parameters; the following information is provided for use by the engineering community:

(1) In the near-geosynchronous region of space, significant levels of spacecraft charging can occur:

(a) between 1900 and 0900 Local Time,
(b) at any distance between R_E = 5.3 and 7.8,
(c) at any magnetic latitude between ± 19°,
(d) at any L-shell value between 5.5 and 8.6, and
(e) for any period the magnetic activity index K_p is 2+ or greater.

Charging can extend outside this region anywhere electron fluxes at energies between ~30 keV and 70 keV exceed 6×10^2 elec/cm^2-sec-sr-eV in a plasma-sheet-type low energy particle environment. (That region of space can not now be totally identified with existing data but may extend in to approximately 2.5 to 3 R_E and out beyond lunar altitudes in the magnetospheric tail under certain magnetic substorm conditions.)

(2) A "worst case" environment can best be described by the first four moments of the distribution function both over the total population from 0 to 400 keV and over the range from 20 keV to 400 keV where charge level is determined. The set of "worst case" moments integrated over pitch angle are:

(a)	total number density:	Ions 3.0,	Electrons 3.0 cm^{-3},
(b)	high number density:	Ions 0.8,	Electrons 0.6 cm^{-3},
(c)	total number flux:	Ions 4×10^8,	Electrons 1.3×10^{10} cm^{-2}-s^{-1},
(d)	high number flux:	Ions 2×10^8,	Electrons 4.9×10^9 cm^{-2}-s^{-1},
(e)	total energy density:	Ions 3.7×10^4,	Electrons 2.4×10^4 eV-cm^{-3},
(f)	high energy density:	Ions 2.8×10^4,	Electrons 1.4×10^4 eV-cm^{-3},
(g)	total energy flux:	Ions 9.4×10^{12},	Electrons 1.9×10^{14} eV-cm^{-2}-s^{-1},
(h)	high energy flux:	Ions 8.3×10^{12},	Electrons 1.5×10^{14} eV-cm^{-2}-s^{-1}.

The total densities for ions and electrons are balanced in a way to maximize charging. High refers to the 20-400 keV range.

(3) If two-Maxwellian fit parameters are required, the following fits will give a maximum realistic charging spectrum parallel and perpendicular to the magnetic field:

(a)	n_1	∥ :	Ions 1.1	Electrons 1.0 cm^{-3},
(b)	n_2	∥ :	Ions 1.7	Electrons 1.5 cm^{-3},
(c)	T_1	∥ :	Ions 0.4	Electrons 0.6 keV,
(d)	T_2	∥ :	Ions 24.7	Electrons 25.1 keV,
(e)	n_1	⊥ :	Ions 0.9	Electrons 0.8 cm^{-3},
(f)	n_2	⊥ :	Ions 1.6	Electrons 1.9 cm^{-3},
(g)	T_1	⊥ :	Ions 0.3	Electrons 0.6 keV,
(h)	T_2	⊥ :	Ions 25.6	Electrons 26.1 keV.

The above spectra are quite isotropic although times of large anisotropies were seen during charging. The degree of anisotropy could affect certain vehicle designs; therefore, if desired, more anisotropy can be simulated by decreasing the parallel component.

Again it should be stressed that the data contain no super substorms. Also, the high energy electron fluxes seen on days 241 and 363 were at lower R_E's and L-shells where the plasma density was quite high. Whether such large fluxes could be produced in a less dense plasma at further R_E's and greater L-shells is not known, and until the dynamics are understood, will not be determinable. However, if high energy electron fluxes as seen on day 241 were present in a less dense plasma environment, ϕ_f would be higher and the probability of adverse effects on a spacecraft increased. Likewise, spacecraft charging increases greatly in satellite eclipse when the photoelectrons are cut off. As was shown in Mullen et al[1], if the higher charging environments which have occurred in sunlight occurred in eclipse, ϕ_f would have reached levels in excess of -15 kV. This level is greater than any charging seen to date on SCATHA.

References

1. Mullen, E.G., Gussenhoven, M.S., and Garrett, H.B. (1981) A "Worst Case" Spacecraft Environment as Observed by SCATHA on 24 April 1979, AFGL-TR-81-0231, AD A108680.

2. DeForest, S.E. (1972) Spacecraft charging at synchronous orbit, JGR, 77:651-659.

3. Stevens, J.R., and Vampola, A.L. (Eds.) (1978) Description of the Space Test Program P78-2 Spacecraft and Payloads, SAMSO-TR-78-24.

4. Mizera, P.F., and Boyd, G.M. (1982) A Summary of Spacecraft Charging Results, AIAA Reprint 82-0286 presented at the AIAA 20th Aerospace Sciences Meeting, January 11-14, 1982, Orlando, Florida.

5. Olson, W.P., and Pfitzer, K.A. (1974) A quantitative model of the magnetospheric field, JGR, 79:3739-3748.


FILMED
9-8